

International Journal of Applied Mathematics in Control Engineering

Journal homepage: <http://www.ijamce.com>

Research on Gas Source Localization Method Based on UAV Olfactory-Visual Fusion

Yu Zhang^a, Lei Cheng^{b,*}^a School of Artificial Intelligence /School of Information Science and Engineering, Wuhan University of Science and Technology, Wuhan, Hubei, 430081, China^b School of Artificial Intelligence /School of Information Science and Engineering, Wuhan University of Science and Technology, Wuhan, Hubei, 430081, China

ARTICLE INFO

Article history:

Received 15 April 2023

Accepted 22 May 2023

Available online 25 May 2023

Keywords:

Gas source localization

Olfactory-visual fusion

Optical gas imaging

Receding horizon Infotaxis

UAV

ABSTRACT

Gas source localization (GSL) is an important task in environmental monitoring and industrial safety. In recent years, UAVs are versatile and autonomous mobile agents that can carry payloads, making them ideal for a wide range of inspection tasks. This paper proposes a gas source localization algorithm for UAVs based on Olfactory-Visual Fusion. The algorithm addresses the challenge of locating gas sources in outdoor time-varying airflow environments. And we build a CFD gas environment and UAV source searching platform, which provides a new solution for tracking UAV odor plumes and locating odor sources in outdoor natural environments.

Published by Y.X.Union. All rights reserved.

1. Introduction

In recent years, with the rapid development of the petrochemical industry, the risks and hazards in this field have also increased, and disasters caused by dangerous gas leaks are particularly severe (Li Lei, 2021). Currently, the petrochemical industry mainly relies on fixed-point sampling and manual inspection to detect leakage points. However, this method has its limitations and cannot perform all-round and high-frequency detection, making it difficult to detect small leaks (Zhu Shengjie, et al. 2020). In addition, leaked hazardous gases may pose a threat to the safety of workers' lives. Therefore, there is an urgent need for a more accurate, efficient, and safer method to determine the location of gas leaks.

Since the 1990s, researchers from around the world have been devoted to the study of olfactory robots. The GSL represents an important application direction in this field. However, these robots often face difficulties in completing tasks due to the presence of suspicious sources or weak wind conditions. In an effort to improve the accuracy and robustness of GSL, some researchers have sought to simulate biological sensing of the external environment and endow mobile robots with vision in order to enhance their functionality (Bian Zhenggang, 2015). Traditional GSL technologies have focused on two-dimensional searches, yet gas diffusion behavior in three-dimensional space presents limitations in robots acquiring accurate gas information. Meanwhile, due to UAV ability to carry various sensors and achieve high-density sampling over large areas, they

have found widespread use in various monitoring tasks. Compared to traditional ground robots, rotary-wing UAVs possess the advantages of high speed, a wide operational range, and reduced interference from terrain (Javier Burgués, et al. 2020) (Francis A, 2022). Moreover, UAVs have advantages over traditional sensor networks in speed of deployment, flexibility, and accuracy (Neumann P P, et al. 2013). Furthermore, after undergoing special processing, UAVs can even function in adverse environments, and can be reused while maintaining higher levels of precision and efficiency. The use of search algorithms and movement strategies in combination with UAVs for GSL has become a major research focus of experts and scholars worldwide.

Building upon the aforementioned research, this paper aims to solve the problem of searching for a single stationary gas plume that continuously emits smoke in a variable outdoor airflow environment for UAV. We propose to fuse vision and olfaction to study the relevant algorithms and strategies for gas plume detection, tracking, and gas source confirmation, forming a complete closed-loop source searching process that effectively enhances the UAV search efficiency and success rate. We have also established a CFD gas environment and UAV searching platform, providing a new solution for outdoor natural environment gas plume tracking and GSL.

2. Methods

2.1 Problem description

The complete closed-loop source-seeking process of an unmanned

* Corresponding author.

E-mail addresses: 932376015@qq.com (Y. Zhang)

doi:

aerial vehicle consists of three stages: smoke plume detection, smoke plume information tracking, and gas source confirmation (Chen X X, et al. 2019). During the smoke plume detection stage, the UAV can be operated either by following a pre-planned trajectory or through manual control. For a fixed detection area, the UAV trajectory should be pre-set to ensure complete coverage in the shortest time and with minimal energy consumption. In a new or small detection area, manual control should be adopted to minimize energy consumption while ensuring complete coverage and obstacle avoidance. At this stage, both olfactory and visual sensors are utilized to search for suspicious smoke plumes.

Three situations exist for smoke plume detection, situation A: visually seeing the smoke plume, situation B: seeing and smelling the smoke plume, and situation C: smelling the smoke plume. Because olfactory and visual searches are mutually independent and cannot work simultaneously, a behavioral decision must be made. In this article, olfactory priority is set higher than visual. When both olfactory and visual sensors detect gas at the same time, the olfactory

search behavior is adopted, and a visual search behavior is used only when the olfactory sensor does not detect anomalies but the visual sensor does, which is shown in Fig. 1.

Plumes have an inherent characteristic during their spread in the air - a high gas concentration and the plume is more concentrated near the gas source (Shen X, et al. 2021). This feature must be utilized in the critical final source-seeking phase to determine the gas source. However, traditional gas source confirmation, which mostly utilises ground mobile robots, relies solely on the high concentration characteristic and typically considers gas concentration above a certain threshold as a gas source. This method has an apparent limitation as it can yield pseudo gas sources and fall into local optima. This study extends the two-dimensional source-seeking to three-dimensional source search based on the UAV platform. Gas source confirmation is markedly improved via detecting the peak changes in gas concentration in 3D space when it reaches the maximum and inspecting the plume source detected by visual sensors. This method significantly enhances the accuracy of gas source confirmation.

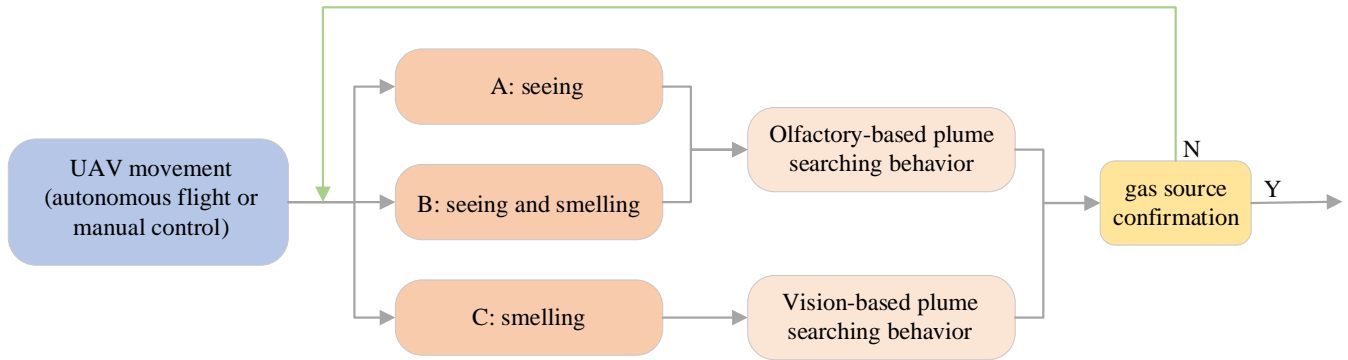


Fig.1. UAV sniffing and fusion gas source search process.

2.2 Olfactory-based searching behavior

Previous algorithms for olfactory source finding typically divide the task into separate subtasks of source finding and obstacle avoidance, making them unsuitable for environments with many obstacles. In this paper, we propose an information-theoretic source search and estimation strategy that integrates source finding and obstacle avoidance based on receding horizon Infotaxis (RHI), a method that plans multi-step forward-looking decisions to find more efficient paths and avoid local optima and obstacles. We also adopt random sampling and a binary sensor model to reduce computational complexity and make the computational load manageable. Our approach minimizes entropy based on information convergence and closely integrates obstacle avoidance and search to enable accurate and robust source term estimation in unknown and complex environments using UAV platforms.

This study assumes that the gas source is fixed at $\mathbf{P}_s = [x_s, y_s, z_s]^T \in \mathbb{R}^{3+}$ and maintains a constant release intensity $I_s \in \mathbb{R}^+$. $\theta = [x_s, y_s, z_s, I_s]^T \in \mathbb{R}^{4+}$ represents the source term vector. μ_k denotes the average gas concentration at the sensing position $\mathbf{P}_k = [x_k, y_k, z_k]^T$ at the k th time step, which is calculated using the dispersion model with the source term vector [17]. c_k represents the measured data of the sensor, and $c_{1:k} = [c_1(\mathbf{p}_1), \dots, c_k(\mathbf{p}_k)]$ is the observation sequence at each sensing position. The UAV is equipped with a laser radar, which can create local maps of unknown obstacle environments. These maps of obstacles are used to generate available paths for the estimation of source item and each step of the UAV

decision satisfies $a \in A = [\uparrow, \downarrow, \leftarrow, \rightarrow, \hat{\uparrow}, \hat{\downarrow}]$.

Based on the sample-based sequential Monte Carlo method-Particle filter, the state of the source term of the highly nonlinear random system was estimated. The samples θ_k collected by the particle filter (called particles) represent the source term, and at the k th time step, each particle $\theta_k^{(i)}$ is extracted from the proposal distribution and its associated weight $w_k^{(i)}$ to approximate the exact source term probability density distribution (PDF) in the Bayesian inference formula, and approximate the subsequent term:

$$p(\theta_k | c_{1:k}) \approx \sum_{i=1}^{N_p} w_k^{(i)} \delta(\theta - \theta_k^{(i)}) \tag{1}$$

where N_p is the number of the particles and δ is the Dirac Delta function. The unnormalized particle weight update based on Bayesian inference can be expressed as:

$$w_k^{(i)} = p(c_k | \theta_k^{(i)}) \cdot w_{k-1}^{(i)} \tag{2}$$

where

$$p(c_k | \theta_k) = \mathcal{N}(c_k; \mu_k, \sigma_k) = \frac{1}{\sigma_k \sqrt{2\pi}} \exp\left[-\frac{(c_k - \mu_k)^2}{2\sigma_k^2}\right] \tag{3}$$

$$\sigma_k \equiv \sqrt{\sigma_{k, \text{sen}}^2 + \sigma_{k, \text{env}}^2} \tag{4}$$

The standard deviation of the environmental noise σ_{env} is constant, while the detection noise σ_{sen} is proportional to the current

background concentration, that is $\sigma_{\text{sen}} \propto \mu_k^i$. The expected PDF of the source term $p(\theta_k | c_{1:k}, \hat{c}_{k+1})$, can also be approximated by a particle filter. The unnormalized weights for updating the potential source term can be calculated:

$$\hat{w}_{k+1}^{(i)} = p(\hat{c}_{k+1}(a_k) | \theta_k^{(i)}) \cdot w_k^{(i)} \quad (5)$$

The normalized weights are

$$\hat{w}_{k+1}^{(i)} = \frac{\hat{w}_{k+1}^{(i)}}{\sum_{j=1}^{N_p} \hat{w}_{k+1}^{(j)}} \quad (6)$$

The probability of a binary measurement at the k th time step $b_k \in [0,1]$ is expressed as

$$p(b_k | \theta) = \begin{cases} \Phi\left(\frac{\bar{b}_k - \mu_k}{\sigma_{\text{env}}}\right) & (b_k = 0) \\ 1 - \Phi\left(\frac{\bar{b}_k - \mu_k}{\sigma_{\text{env}}}\right) & (b_k = 1) \end{cases} \quad (7)$$

where

$$\bar{b}_k = \begin{cases} \lambda_b \bar{b}_{k-1} + (1 - \lambda_b) c_k & (k > 1, c_k > \bar{b}_{k-1}) \\ \bar{b}_{k-1} & (k > 1, c_k \leq \bar{b}_{k-1}) \\ c_k & (k = 1) \end{cases} \quad (8)$$

where λ_b is the user design parameter. $\mathbf{b}_{k+1:k+n-1}^{(m)} = [\hat{b}_{k+1}^{(m)}, \hat{b}_{k+2}^{(m)}, \dots, \hat{b}_{k+n-1}^{(m)}]$ is the future measurement set of binary sensors, and each component of the future measurement series predicted at the $(k+n)$ th time step $\hat{b}_{k+n}^{(m)}$ from the estimated source term distribution $P(\hat{b}_{k+n}^{(m)} | c_{1:k}, \mathbf{b}_{k+1:k+n-1}^{(m)})$, which is approximated by the particle filter as:

$$\hat{b}_{k+n}^{(m)} \sim p(\hat{b}_{k+n}^{(m)} | c_{1:k}, \mathbf{b}_{k+1:k+n-1}^{(m)}) = \sum_{i=1}^{N_p} p(\hat{b}_{k+n}^{(m)} | \theta_k^{(i)}) \hat{w}_{k+n-1}^{(i)} \quad (9)$$

To reduce computational complexity, a random sampling method was employed, and only a small number of sampled future measurement sequences from the estimated source probability distribution are considered instead of all possible future measurement orders in the receding horizon step. The mobile sensor selects the optimal decision sequence of a specific time range with length K at time-step k , $\hat{a}_{k:k+K-1} = [\hat{a}_k, \hat{a}_{k+1}, \dots, \hat{a}_{k+K-1}]$.

The reduction of entropy for each source term at each time step is estimated using a utility function:

$$U(a_{k:k+K-1}^{\text{path}}) = \sum_{n=1}^K r^n \sum_{m=1}^{N_m} \frac{U_{k+n-1}^{\text{path}}}{N_m} \quad (10)$$

where

$$U_{k+n-1}^{\text{path},m} = - \sum_{i=1}^{N_p} \hat{w}_{k+n-1}^{(i)} \log \hat{w}_{k+n-1}^{(i)} + \sum_{\hat{b}_{k+n}=0}^1 p(\hat{b}_{k+n} | \theta_k) \sum_{j=1}^{N_p} \hat{w}_{k+n}^{(j)} \log \hat{w}_{k+n}^{(j)} \quad (11)$$

N_p denotes the number of particles of the particle filter (potential source term). m denotes the m th sample of future measurements that can be obtained from the sample of decision sequences along the path. We are less confident in the utility function for further predictions and introduce a confidence ratio of $0 \leq r \leq 1$ as a discount factor. The information convergence strategy guides the mobile sensor to obtain measurements in the direction that minimizes the expected entropy of the potential source term PDF. Therefore, we choose the optimal decision to maximize the utility function.

$$a_{k:k+K-1}^* = \arg \max_{a_{k:k+K-1}^{\text{path}} \in A_{k:k+K-1}} U(a_{k:k+K-1}^{\text{path}}) \quad (12)$$

Due to the inaccurate prediction of the future, we use only the first element a_k^* of the optimal decision sequence for the actual moving.

Algorithm: pseudocode of the algorithm RHI at step k

```

1: Get new data from olfactory sensors  $c_k$ 
2: Update the obstacle map
3: Update the particle source term using particle filtering
   ( $\theta_{k-1}^{(i)}, w_{k-1}^{(i)} \rightarrow (\theta_k^{(i)}, w_k^{(i)})$ )
4: for  $path = 1, \dots, 6^K$  (over-prediction of all decision paths generated)
5:   for  $m = 1, \dots, N_m$ 
     ( $N_m$  sequences selected among the  $N_d$  discrete measurement
      sequences generated by the measurement)
6:     for  $n = 1, \dots, K$  ( $K$  step path for UAV)
7:       if no obstacles ahead
8:         Update measurements  $\hat{b}_{k+1:k+n-1}^{(m)}$ 
9:         Calculate the utility function for this step  $U_{k+n-1}^{\text{path},m}$ 
10:      else
11:        Break
12:     end
13:   end
14: Calculate  $U(a_{k:k+K-1}^{\text{path}})$ 
15: end
16: Choose the best path  $a_{k:k+K-1}^*$ 
17: Move to a new sensing position
18:  $\mathbf{P}_k = [x_k, y_k, z_k]^T \rightarrow \mathbf{P}_{k+1} = [x_{k+1}, y_{k+1}, z_{k+1}]^T$ 
    
```

2.3 Vision-based plume searching behavior

In the petroleum and chemical industry, most gas leaks are not visible to the naked eye. However, the emergence of Optical Gas Imaging (OGI) has changed this situation by enabling the visualization and accurate positioning of leaks that are not visible to the naked eye, especially volatile organic compound (VOC) leaks. OGI enables rapid and efficient visualization detection of gas leaks, avoiding the risk of exposure to toxic gases for detection personnel, and quickly scanning equipment components to eliminate safety hazards. However, OGI still has limitations, such as restricted detection range and blind spots. Moreover, OGI detection relies on operator judgment and generally lacks real-time feedback.

To address the limitations of OGI, mounting OGI on unmanned aerial vehicles (UAVs) can achieve comprehensive and multi-angle scanning and inspection. In 2015, Ren Shaoqing proposed Faster R-CNN (Ren Shaoqing, et. 2021), which achieved real-time detection of targets. Faster R-CNN is an improved version of R-CNN and Fast R-CNN, with faster and more accurate target detection capabilities. Faster R-CNN is based on a deep neural network that implements target detection and comprises two main components: the Region Proposal Network (RPN) and the Fast R-CNN detector. RPN is an algorithm that uses convolutional neural networks to quickly generate candidate regions and can quickly detect possible target regions in the original image. The Fast R-CNN detector is used to further detect targets in candidate regions by extracting features, performing classification and regression in each candidate region to identify and locate targets. Compared with previous target detection algorithms, Faster R-CNN does not require manual feature extraction, but instead automatically learns features through deep neural network training. This method not only improves detection accuracy, but is

also more flexible and easier to implement.

RPN achieves object detection by first examining which position in the feature map contains the object through the classifier, and then adjusting the corresponding position accordingly through the regressor. In order to generate region proposals for the CNN-based detection network, the classifier and regressor are trained according to the following equations, ultimately detecting the object's class and region.

The loss function is:

$$L(\{p_i\}, \{t_i\}) = \frac{1}{N_{cls}} \sum_i L_{cls}(p_i, p_i^*) + \lambda \frac{1}{N_{reg}} \sum_i p_i^* L_{reg}(t_i, t_i^*) \quad (13)$$

Where i represents the index of an anchor in a mini-batch. p_i is the predicted probability that anchor i contains an object. p_i^* represents the ground truth label, which is 1 if the anchor is positive and 0 if it is negative. t_i is the vector that predicts the 4 parameterized coordinates of the bounding box, and t_i^* is the ground-truth box associated with the positive anchor. The formula consists of two main parts: the classification loss L_{cls} is used to train the network to classify anchors as positive or negative, and the regression loss L_{reg} is used for bounding box regression training. The two parts in the formula are normalized using N_{cls} and N_{reg} , and the latter incorporates a balance weight λ . For the regression loss, a robust loss function ($smooth_{L1}$) is used, which is defined as follows:

$$L_{reg}(t_i, t_i^*) = \sum_{i \in \{x, y, w, h\}} smooth_{L1}(t_i - t_i^*) \quad (14)$$

$$smooth_{L1}(x) = \begin{cases} 0.5x^2 & (|x| < 1) \\ |x| - 0.5 & (\text{otherwise}) \end{cases} \quad (15)$$

where the four-dimensional vector x , y , w , and h represent the center coordinates and width and height of the window.

Based on the collected gas target data, including sample images and labeling information of different types of gases, the Faster R-CNN algorithm is used for training to obtain the Faster R-CNN model. During formal detection, the trained Faster R-CNN model is used to detect the target in the input image. In the detection process, the sliding window and region of interest methods are used to extract and classify the possible gas target regions in the image, and the final target detection results are outputted. At this stage, the UAV adjusts its direction based on the target's position in the field of view. When the target is on the left side of the field of view, the UAV moves to the left, and when the target is on the right side of the field of view, the UAV moves to right, always keeping the target in the center of the UAV field of view. When the UAV approaches the target, it can be determined whether the target is a plume source. If it is a plume source, the UAV releases the source position. During the search, if the smell sensor senses the gas, the smell-based search behavior is executed.

3. Results

This section describes the scenario of gas diffusion in a three-dimensional environment rich in obstacles. The search area is $300m \times 300m \times 6m$. The standard deviation of the environmental noise $\sigma_{env} = 0.4mg / m^3$, the detection noise $\sigma_{sen} = 0.2\mu(p; \theta)$, the binary sensor model threshold update parameter $\lambda_b = 0.7$, the

confidence ratio $r = 0.7$, the number of samples of the future measurement sequence, and the number of particles for the particle filter $N_p = 500$.

Tab. 1. Gas source information and obstacle distribution.

ID	$\mathbf{P}_s = [x_s, y_s, z_s]^T$	I_s	pseudo-gas source	η
(a)	(190.0, 225.0, 2.0)	4mL/min		less
(b)	(190.0, 225.0, 2.0)	4mL/min	(175.4, 152.1, 3.24)	less
(c)	(175.0, 200.0, 2.0)	4mL/min		more
(d)	(200.0, 235.0, 2.0)	4mL/min	(181.3, 158.6, 2.89)	more

Table 1 describes the initial gas source setup and the number of obstacles, where η denotes the degree of how many obstacles are present.

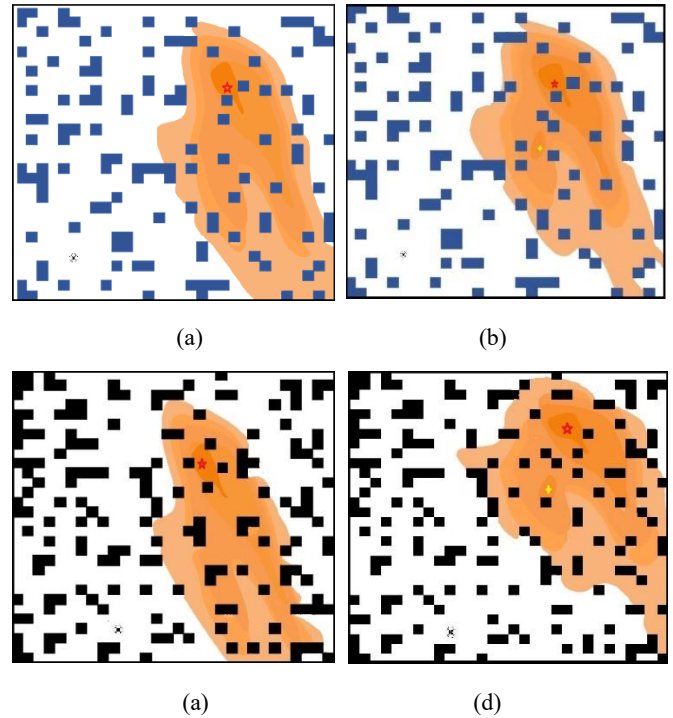


Fig. 2. Figure (a), (b), (c), (d) correspond to the four sets of experiments, where the blue and black boxes represent obstacles and the rest of the area represents the UAV-accessible area. Different shades of color represent different gas concentrations. The red pentagram indicates the location of the gas source, and the yellow four-pointed star indicates the pseudo-gas source.

Four sets of experiments were conducted under different conditions of obstacle quantity and the presence of false gas sources, as shown in Fig. 2. At the beginning of the experiment, the UAV was positioned outside the gas diffusion area and could not detect the presence of gas through the gas sensor, but the plume was identified through OGI, as shown in Fig. 3. At this point, the UAV executed a vision-based search behavior and quickly approached the plume. When the plume was reached, the olfactory sensor detected the presence of gas, and the UAV stopped the vision-based search behavior and switched to an olfaction-based search behavior until the gas source was found. According to the data in the table, it can be seen that the presence of false gas sources under the same obstacle quantity condition can cause some difficulty in determination, but the UAV can still move towards the real gas source in a short period of time. In addition, obstacle quantity affects the speed of UAV movement, but the UAV is still able to avoid obstacles and complete the search task.



Fig. 3. OGI visualizes the gas into a grayscale image and labels the gas with a Faster R-CNN model for target detection.

Tab. 2. Data of the gas search process.

ID	Start position	Source declaration location	Error	Time step
1	(60.0, 45.0, 0.0)	(189.3, 225.7, 1.95)	0.99	35
2	(60.0, 45.0, 0.0)	(189.1, 224.5, 1.96)	1.03	48
3	(100.0, 35.0, 0.0)	(173.9, 201.1, 1.95)	1.56	37
4	(100.0, 35.0, 0.0)	(198.3, 234.1, 1.93)	1.92	55

4. Summary

The olfactory vision fusion technology based on UAV platform can better accomplish the task of gas source determination, visualize the gas through OGI, which makes it possible to find the plume at a longer distance, improve the efficiency of finding the plume and avoid blind search, while combining with olfactory sensors in gas source determination to enhance the accuracy of gas source localization and solve the problem of gas source localization caused by pseudo-gas sources in turbulent environment. Meanwhile, the UAV makes the traditional gas source finding change from two-dimensional to three-dimensional, making full use of the spatial concentration characteristics of the gas source in three dimensions, as well as improving the source finding limitations due to other factors such as terrain. In order to solve the difficulty of obstacle avoidance in the source finding process, the backward view greedy algorithm is used to combine source finding and obstacle avoidance and reduce the computational load of real-time decision making using random sampling and binary sensor model. However, there are still some areas for improvement. Firstly, the feasible decision of UAV can be extended to two or even three directional vectors and improve the search efficiency. Secondly, the grayscale image formed by using OGI is blurred to a large extent, and in the process of real-time recognition, the image needs to be enhanced and segmented, and the

computational complexity and recognition is difficult, so the visual target detection method needs to be improved.

References

- Li Lei, 2021. Simulation and analysis of typical fire accidents in petrochemical tank farm[J]. Journal of Beijing University of Chemical Technology (Natural Science Edition). 48(2): 23-30
- Zhu Shengjie, Ding Dewu, Wang Guolong, et al, 2020. Research on volatile organic compounds leakage detection technology in petrochemical enterprises. Safety Health & Environment. 20(8):1-5.
- Bian Zhenggang. Robotics and automation technology, 2015. Automation Panorama. 2015(3): 76-78.
- avier Burgués, Santiago Marco, 2020. Environmental chemical sensing using small drones: A review. Science of The Total Environment. 748:141-172
- Adam Francis, Shuai Li, Christian Griffiths, et al, 2022. Gas source localization and mapping with mobile robots: A review. Journal of Field Robotics. 39(8):1341-1373
- Patrick P. Neumann, Victor Hernandez Bennetts, Achim J. Lilienthal, et al, 2013. Gas source localization with a micro-drone using bio-inspired and particle filter-based algorithms. Advanced Robotics. 27:9, 725-738.
- Chen Xin-xing, Chen Jian Huang. Odor source localization algorithms on mobile robots: A review and future outlook, 2019. Robotics and Autonomous Systems. 112:123-136
- Shen Xiangyuan, Yuan Jie, Shan Yugang, 2021. A novel plume tracking method in partial 3D diffusive environments using Multi-sensor fusion. Expert Systems with Applications. 178(1): 114993.
- Ren Shaoqing, He Kaiming, Girshick Ross, et al, 2015. Faster R-CNN: Towards Real-Time Object Detection with Region Proposal Networks. 28.



Yu Zhang is currently pursuing a master's degree in the School of Information Science and Engineering at Wuhan University of Science and Technology (WUST). she received her bachelor's degree from WUST in 2022. Her research interests include machine learning, robot olfaction.



Lei Cheng is currently a professor at Wuhan University of Science and Technology and a joint doctoral tutor at the University of the West of England. He is a member of the Intelligent Robotics Committee of the Chinese Society of Artificial Intelligence. He received his Ph.D. from Huazhong University of Science and Technology in 2005. The main research direction is machine smell, multi-subject and robot control.